Electronic, elastic, vibrational, and thermodynamic properties of type-VIII clathrates Ba8Ga16Sn30 and Ba8Al16Sn30 by first principles

Payam Norouzzadeh, Charles W. Myles, and Daryoosh Vashaee

Citation: Journal of Applied Physics **114**, 163509 (2013); doi: 10.1063/1.4826213
View online: http://dx.doi.org/10.1063/1.4826213
View Table of Contents: http://scitation.aip.org/content/aip/journal/jap/114/16?ver=pdfcov
Published by the AIP Publishing

Electronic, elastic, vibrational, and thermodynamic properties of type-VIII clathrates $Ba_8Ga_{16}Sn_{30}$ and $Ba_8Al_{16}Sn_{30}$ by first principles

Payam Norouzzadeh,[1] Charles W. Myles,[2] and Daryoosh Vashaee[1,a)]
[1]*School of Electrical and Computer Engineering, Helmerich Advanced Technology Research Center, Oklahoma State University, Tulsa, Oklahoma 74106, USA*
[2]*Department of Physics, Texas Tech University, Lubbock, Texas 79409-1051, USA*

(Received 4 September 2013; accepted 3 October 2013; published online 24 October 2013)

We present the results of studying electronic, elastic, vibrational, and thermodynamic properties of type-VIII clathrates $Ba_8Ga_{16}Sn_{30}$ $Ba_8Al_{16}Sn_{30}$ calculated from a first-principles approach. The calculations utilize the generalized gradient approximation to density functional theory. The results indicate that the $Ba_8Ga_{16}Sn_{30}$ and $Ba_8Al_{16}Sn_{30}$ are indirect semiconductors with fundamental band gaps of 160 meV and 315 meV, respectively. It was also found that the stiffness of Al containing type-VIII clathrate does not show any significant change against the uniform pressure, shearing, and linear strains. The phonon spectrum and the phonon state densities of these compounds as well as the Raman and infrared active modes were further calculated and the effects of replacing the Ga with Al atoms on the properties of interest were discussed. The calculated elastic, vibrational, and thermodynamic properties along with Raman and IR spectra are reported for the first time. The identification of the Raman and infrared active modes will be especially useful for the experimental characterizations of these compounds. Our calculations show that the heat capacities of these clathrates increase smoothly with temperature and approach the Dulong-Petit value at about room temperature, which agrees with the existing experimental data. © *2013 AIP Publishing LLC*. [http://dx.doi.org/10.1063/1.4826213]

I. INTRODUCTION

The clathrate compounds have been studied mainly due to their promising thermoelectric (TE) properties.[1–3] Nevertheless, a range of other rich physical properties for these compounds, such as mechanical,[4] superconductivity,[5,6] and magnetic[7] properties have been investigated extensively. With the increasing interest in thermoelectric technology for power generation, cooling, or sensing and imaging applications, new materials, devices, and characterization techniques are being developed.[8–10] At present, the best thermoelectric materials are degenerate or near degenerate semiconductors with low thermal conductivities. Several methods based on nanostructuring,[11–13] energy filtering techniques,[14–16] low dimensional structures,[17,18] resonant energy levels,[19] embedded nano-inclusions,[20,21] and complex material systems[22] have been developed to improve the thermoelectric properties of materials. The concept of phonon-glass electron crystal (PGEC) indicates that the low lattice thermal conductivity and high electrical conductivity are required to obtain excellent TE properties.[23] Of the several classes of materials which have been studied for such properties, several clathrate compounds have been shown to be promising candidates.[8] Vibrations, or the so called rattling, of guest atoms inside the framework of the clathrate compounds at much lower frequencies than that of the host atoms are believed to scatter the acoustic phonons of the framework atoms; hence, reducing the lattice thermal conductivity.[1,24] While the guest atoms reduce the thermal conductivity, they usually have little effect on the electrical properties, which explains why clathrates are potentially good candidates to fulfill the PGEC concept.

The electronic, vibrational, magnetic, and TE properties of Si-, Ge-, Sn-based clathrates have been studied extensively in the past.[1,2,25,26] The Sn-based clathrates, due to the heavier Sn atoms and larger framework size than that of Si or Ge based clathrates, appear to be more promising TE materials for moderate-temperature applications.[27] As such, the electrical and thermal transport properties of tin based clathrates have been investigated both empirically and theoretically by several research groups.[2,3,28–37]

The type-VIII clathrate structure is believed to provide high charge carrier mobility in general.[28] Until now, only six compounds of $Ba_8Ga_{16}Ge_{30}$,[38] $Eu_8Ga_{16}Ge_{30}$,[39] $Sr_8Ga_{16-x}Al_xGe_{30}(6 < x < 10)$,[40] $Sr_8Ga_{16-x}Al_xSi_{30}(8 < x < 10)$,[41] $Ba_8Ga_{16-x}Cu_xSn_{30}$ $(0 < x < 0.033)$,[42] and $Ba_8Ga_{16-x}Al_xSn_{30}(0 \le x \le 12)$ (Ref. 43) have been identified in the type-VIII clathrates family (i.e., space group I-43m). From these, transformation to β phase or type-I clathrate (i.e., space group pm-3n) has been reported for the first one above 696C.[44]

The results of a first-principles theoretical study of the electronic, vibrational, elastic, and thermodynamic properties of the type-VIII clathrate $Ba_8Ga_{16}Sn_{30}$ are presented and, in particular, the effect of Al substitution for Ga is taken into account. To the best of our knowledge, no quantitative theoretical study has yet been reported for the elastic, vibrational and thermodynamic properties of $Ba_8Ga_{16}Sn_{30}$-VIII and $Ba_8Al_{16}Sn_{30}$-VIII. The vibrational modes, the phonon state densities, the Debye temperatures and the thermodynamic properties of these compounds were also calculated and presented.

a)Author to whom correspondence should be addressed. Electronic mail: daryoosh.vashaee@okstate.edu. Tel.: +1 918 594 8017.

II. THEORETICAL DETAILS

A. Computational approach

A first-principles density functional plane wave method was applied for the calculations.[45,46] The calculations utilize the generalized gradient approximation (GGA) to density functional theory (DFT). The electron exchange correlation energy is approximated with the Perdew-Burke-Ernzerhof functional.[47] The ultrasoft pseudopotentials are used in this study to approximate the effects of the core and semicore electrons.[48,49] Spin-orbit coupling can split degenerate electronic states; however, due to its relatively small effect on binding energies, we have neglected it in our calculations. The energy cutoff for the plane wave basis was set to 375 eV and the Brillouin zone integration calculations were performed over a $4\times4\times4$ Monkhorst-Pack k-point grid.[50] To minimize the errors in the calculation of the forces, the total energy was converged within 10^{-6} eV. Since the clathrate unit cell is large (54 atoms), only a single unit cell was employed in the calculations. For each compound, we optimized the geometry of each structure. Structural optimization was performed by relaxing the internal coordinates to determine the forces and the energies in the lattice. In order to find the equilibrium lattice constant, we started with a fixed unit cell volume and relaxed the ionic positions by minimizing the total energy through a conjugate gradient algorithm by using atomic forces. This process was repeated for several unit cell volumes, and the energy versus volume data was fit with Birch-Murnaghan equation of state to determine the equilibrium lattice constant, formation energy, and the bulk modulus.[51,52] Finally, the internal coordinates were optimized according to the volume of the minimum energy configuration. The equilibrium structural parameters, the electronic band structures, and the densities of states and all of the other reported quantities were evaluated at the minimum energy configurations.

The three elastic moduli C_{11}, C_{12}, and C_{44} fully describe the elastic behavior of a cubic crystal. C_{11} and C_{12} were obtained from the bulk modulus B and shear constant C_s,

$$B=\frac{C_{11}+2C_{12}}{3} \tag{1}$$

and

$$C_s=\frac{C_{11}-C_{12}}{2}. \tag{2}$$

The following strains were applied to obtain C_s:[53]

$$\varepsilon=\begin{pmatrix}\delta & 0 & 0\\ 0 & \delta & 0\\ 0 & 0 & (1+\delta)^{-2}-1\end{pmatrix}, \tag{3}$$

where δ is the magnitude of the strain. The Helmholtz free energy of the strained structure $F(\delta)$ is related to δ as $F(\delta)=F(0)+6C_sV\delta^2+O(\delta^3)$ in which V and $F(0)$ are the volume and the free energy of the unstrained structure, respectively. C_{44} is determined by applying the following stress:[37]

$$\varepsilon=\begin{pmatrix}0 & \delta & 0\\ \delta & 0 & 0\\ 0 & 0 & \delta^2/(1-\delta^2)\end{pmatrix}, \tag{4}$$

where the free energy is obtained as $F(\delta)=F(0)+2C_{44}V\delta^2+O(\delta^4)$. The shear modulus G is determined as the solution of Hershey-Kroner relation.[54,55] The shear modulus can be calculated by the Hill polycrystalline modulus[56] $G_H=1/2\,(G_R+G_V)$ in which the G_R and G_V are[57]

$$G_R^{-1}=\frac{2}{5}C'^{-1}+\frac{3}{5}C_{44}^{-1} \tag{5}$$

and

$$G_V=\frac{2}{5}C'+\frac{3}{5}C_{44}. \tag{6}$$

The Young's modulus E can be expressed as

$$E=\frac{9BG}{3B+G} \tag{7}$$

and the longitudinal v_L and the transversal v_T sound velocities were calculated using the following relations, respectively,[58]

$$v_L=\sqrt{\frac{B+4/3G}{\rho}} \tag{8}$$

and

$$v_T=\sqrt{\frac{G}{\rho}}, \tag{9}$$

where ρ is the density. The average speed of sound was obtained from

$$v_s^{-3}=\frac{1}{3}\left(\frac{1}{v_L^3}+\frac{2}{v_T^3}\right). \tag{10}$$

Given the longitudinal and transversal velocities, the Debye temperature was calculated from[59]

$$\theta_D=\frac{hv_s}{k_B}\left[\frac{3}{4\pi}\left(\frac{N_A\rho}{M}\right)\right]^{\frac{1}{3}}, \tag{11}$$

where h, k_B, N_A, and M, are Planck's constant, Boltzmann's constant, Avogadro's number, and average molecular weight, respectively.

To carry out the calculations of the phonon dispersion and the thermodynamic properties including the heat capacity, the free energy and the entropy changes, we employed the Phonon software package in which the direct method is applied.[60] The zero-point energy and the phonon free energy changes were obtained and used for analyzing the thermodynamic stabilities. In phonon calculations, for each compound, we selected the optimized unit cell that was calculated through GGA-DFT in the previous step. Then a

set of displaced supercells was generated with the displacement of ± 0.02 Å of the nonequivalent atoms. The set contained 15 different displaced supercells which were extended equally in all directions (5 in each direction) without reducing the symmetry of the system. The DFT calculations were repeated for each displaced supercell to obtain the force on each atom due to the corresponding displacements. The calculated forces were returned to the PHONON software[42] to determine the phonon dispersion curves and the vibrational density of states. The thermodynamic properties of the selected compounds were evaluated at a given range of temperature using the partition functions extracted from the phonon dispersions and the vibrational densities of states.[61,62]

The thermodynamic properties of the clathrates of interest were calculated assuming that (1) the system is a perfect crystalline lattice, (2) the only contribution to the entropy is due to the lattice vibrations, (3) the harmonic approximation is valid, and (4) the anharmonicity is negligible because all the vibrational eigenvalues were obtained at $T = 0$ K. The vibrational Helmholtz free energy (F_{vib}), the vibrational entropy (S_{vib}) and the specific heat at constant volume (C_V) were calculated from the vibrational density of states (VDOS). The procedure to obtain the VDOS is outlined elsewhere.[63]

Experimental characterizations are typically performed at constant pressure; nevertheless, it is fairly accurate to calculate the Helmholtz free energy rather than the Gibbs free energy in an ambient pressure because the volume change is negligible. For simplicity, we assumed the equilibrium volumes in all the calculations. This assumption is justified since the thermal expansion coefficients of semiconductors are generally small up to a few hundred degrees above the room temperature (RT). For example, the thermal expansion coefficient of Si (diamond structure) is 4.68×10^{-6} K^{-1} at RT. The vibrational Helmholtz free energy in the harmonic approximation is given by

$$F_{vib}(T) = k_B T \int_0^\infty \left[\frac{1}{2}\hbar\omega + k_B T \ln\left(1 - e^{-\frac{\hbar\omega}{k_B T}}\right)\right] g(\omega) d\omega. \quad (12)$$

The VDOS is normalized to fulfill $\int g(\omega)d\omega = 3N$ condition, in which N is the number of atoms in the unit cell. The zero point vibrational energy is defined by F_{vib} at $T = 0$ K. The vibrational entropy and specific heat at constant volume are given by

$$S_{vib}(T) = \left(\frac{\partial F_{vib}}{\partial T}\right)_V \text{ and } C_V(T) = -T\left(\frac{\partial^2 F_{vib}}{\partial T^2}\right)_V. \quad (13)$$

B. Crystal structure

Clathrate compounds are comprised of face-shared polyhedral frameworks formed by the group IV elements Si, Ge, and Sn and may be filled with alkali-metal, alkaline-earth or rare-earth elements. The pristine and guest-containing Group IV clathrates and the compounds with some host atom substitutions are all technologically interesting. In the compounds, the choices of the guest atoms and the type and number of the Group II or Group III atoms substituted on the framework may both be used to adjust the physical properties of the compound. Such choices offer a broad spectrum of possible electrical and thermal transport properties for these materials. For example, depending on the host composition and on the choice of the guest atom, the Si-based clathrates can make wide-gap semiconductors,[64] materials with metallic conduction,[65] or superconductors.[66]

The $Ba_8Ga_{16}Sn_{30}$ exists in two phases, α-phase with space group I-43m (No. 217) and the structure of type-VIII clathrate,[67] and β-phase with space group Pm-3n (No. 223) and the structure of type-I clathrate.[3] The same structures are expected for $Ba_8Al_{16}Sn_{30}$. The structural relationship and the description of the phase transformation between the type-I and the type-VIII structure have been reported for the clathrate $Eu_8Ga_{16}Ge_{30}$.[68] The formula of the ideal type-VIII clathrate structure is $A_8B_yC_{46-y}$ in which A atoms are the guest atoms and B or C atoms are the cage or framework atoms. In type-VIII clathrates, the host atom is bonded with 4 neighbor atoms by the *sp*3 hybridizing orbitals and its structure has only one type of dodecahedral cage. The guest atoms (Ba) are encapsulated in the cages consisting of 23 atoms of Ga (Al) and Sn. Guest atoms occupy the 8c Wyckoff positions while the host atoms occupy four Wyckoff sites, 2a, 12d, 8c, and 24g as shown in Figure 1. Among many possible structures of type-VIII clathrates, due to the occupancy of the cage sites, we adopted the configuration with no Al-Al bonds which are similar to the lowest-energy configuration for type-VIII clathrate $Ba_8Ga_{16}Si_{30}$ found by Ross *et al.*[69] In fact, we have assumed that the no Al-Al bond configuration is the most energetically favorable one, which is similar to the previously reported Ba-Al-Ge and Ba-Ga-Ge compounds. The lowest energy configuration of $Ba_8Ga_{16}Sn_{30}$-VIII is obtained when the number of Ga atoms that occupy 8c, 12d, and 24g Wyckoff sites are 8, 8, and 0, respectively.[16] We follow a similar procedure for $Ba_8Al_{16}Sn_{30}$-VIII. It has been shown for these types of semiconducting clathrates that group III elements avoid bonding to each other due to the Coulomb repulsive interactions.[70,71] Guest-guest bonds are unlikely in these compounds because the average distance between the guests is ~5.5 Å, which is almost five times larger than the ionic radius of Ba 1.35 Å.

III. RESULTS AND DISCUSSIONS

A. Electronic and structural properties

The calculated lattice constants derived after the structural optimizations are 11.93 Å and 11.92 Å for $Ba_8Ga_{16}Sn_{30}$-VIII and $Ba_8Al_{16}Sn_{30}$-VIII compounds, respectively. These values indicate that Al atom substitution for Ga atoms in the framework leads to slightly smaller lattice constant which is understandable due to the stronger bonding of Al elements with respect to that of Ga elements. The reported empirical value of the lattice constant of $Ba_8Ga_{16}Sn_{30}$-VIII is 11.58 Å which is ~3% smaller than the calculated value. It is well known that the Local Density Approximation (LDA) underestimates the equilibrium lattice constant by 1%–3%, and the GGA tends to overestimate it by 1%–3% larger than the experimental values.[72] Figure 2 represents complex band

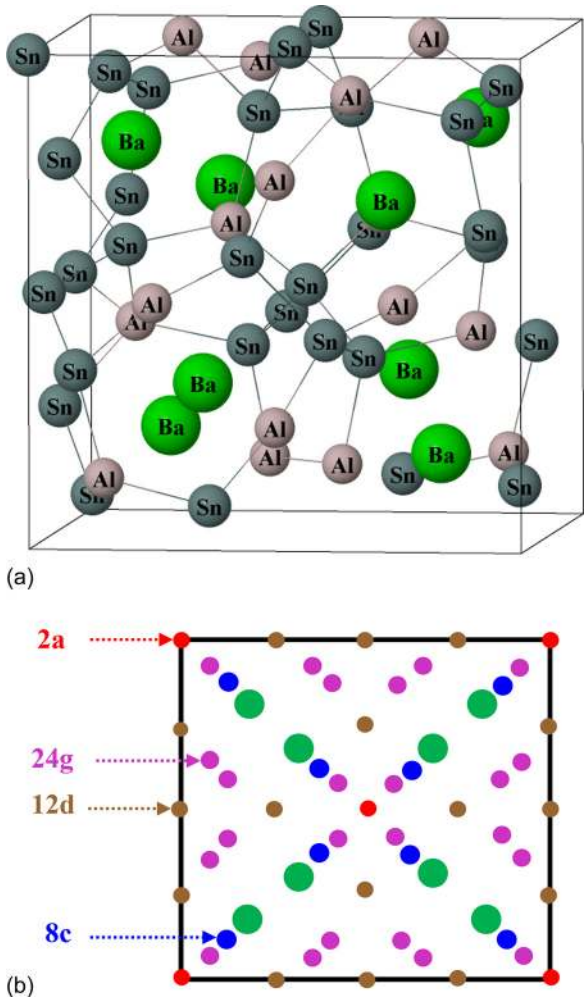

FIG. 1. (a) Crystal structure of a configuration of type-VIII clathrate $Ba_8Al_{16}Sn_{30}$. (b) Representation of Wyckoff sites in a typical type-VIII clathrate. The guest atoms (Ba) occupy 8c sites and the host atoms (Sn and Al/Ga) occupy 2a, 12d, 8c, and 24g sites.

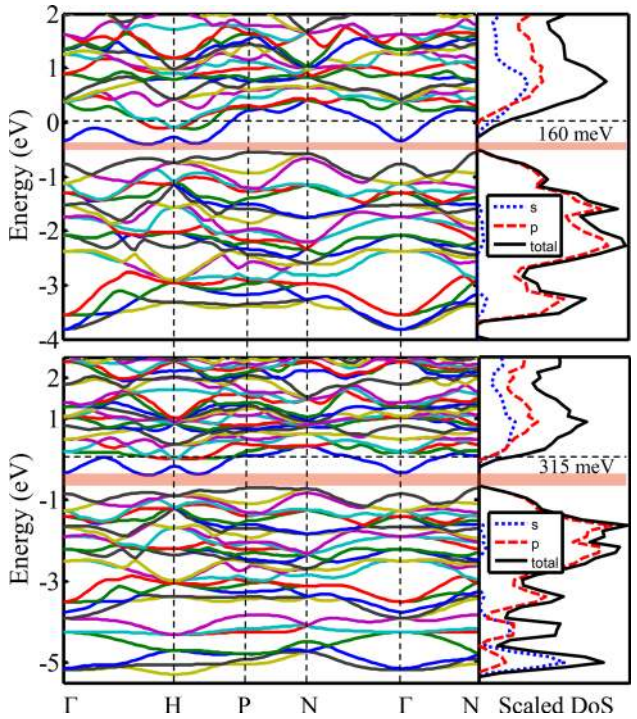

FIG. 2. GGA electronic band structures along with scaled s-orbital projected, p-orbital projected, and total scaled density of states for (a) $Ba_8Ga_{16}Sn_{30}$ and (b) $Ba_8Al_{16}Sn_{30}$. The k-points correspond to $\Gamma = (0, 0, 0)$, $H = (1/2, 1/2, -1/2)$, $N = (1/2, 0, 0)$ and $P = (1/4, 1/4, 1/4)$ in units of $2\pi/a$. The Fermi level is set to 0 eV and is indicated by horizontal dashed line.

structures for the selected compounds which can be attributed to the large number of atoms, and in turn the large number of bands in the unit cell. The flatness of the bands especially near the Fermi level in these compounds makes it difficult to determine the k-point to k-point transition to find the minimum energy gap. Our calculations show that the $Ba_8Ga_{16}Sn_{30}$-VIII and $Ba_8Al_{16}Sn_{30}$-VIII have an indirect band gap between the Brillouin zone points $N = (1/2, 0, 0)$ in the valence band and a k point between $\Gamma = (0, 0, 0)$ and $H = (1/2, 1/2, -1/2)$ points in the conduction band which is almost located at $(3/8, 3/8, -3/8)$. The predicted fundamental GGA band gap of $Ba_8Ga_{16}Sn_{30}$-VIII and $Ba_8Al_{16}Sn_{30}$-VIII compounds are about 160 meV and 315 meV, respectively. It is notable that LDA and GGA density functionals usually underestimate the band gaps of semiconductors. These values show that replacing Ga atoms with Al in $Ba_8Ga_{16}Sn_{30}$-VIII increases the band gap.

The comparison of the calculated band structures shows little modifications in many states near the valence band maxima and the conduction band minima due to the Al substitution for Ga. Figures 2(a) and 2(b) also include the calculation results for the scaled s and p-orbital projected and scaled total electronic density of states (DoS) for each compound of interest. For the selected compounds, the electronic DoS plots are qualitatively similar to each other. It clearly shows that in regions lower than Fermi level the *p*-orbital character is dominant for both compounds while in regions higher than Fermi level, both *s* and *p* orbitals contribute in total density of states. The electronic states of the valence electrons are composed of hybrid sp^3 orbitals and the major contributions to these states originate from the *p* orbitals. In case of $Ba_8Al_{16}Sn_{30}$-VIII the *s* orbitals make a peak around −5 eV. Additionally, we have calculated the total formation energies E_f for $Ba_8Ga_{16}Sn_{30}$-VIII and $Ba_8Al_{16}Sn_{30}$-VIII compounds. The formation energy was calculated from the equation,

$$E_f(Ba_8Ga_{16}Sn_{30}) = E_{Ba_8Ga_{16}Sn_{30}} - 8E_{Ba} - 16E_{Ga} - 30E_{Sn}, \quad (14)$$

where E_{Ba} is the energy per Ba atom in Ba metal, and similarly for the other atoms. This formula was also applied to $Ba_8Al_{16}Sn_{30}$-VIII by replacing the Ga atoms with Al in Eq. (12). The formation energy determines if it is energetically favorable for a material to form in comparison with the solid formed by its constituent elements (Ba, Ga(Al), Sn). We found that the formation energies for $Ba_8Ga_{16}Sn_{30}$-VIII and $Ba_8Al_{16}Sn_{30}$-VIII are −690 and −55.96 kJ/mol per unit cell, respectively. These results indicate that the $Ba_8Ga_{16}Sn_{30}$-VIII and $Ba_8Al_{16}Sn_{30}$-VIII clathrates are thermodynamically more stable than their isolated bulk constituents; therefore, their chemical reaction of formation is exothermic. The calculated formation energies also show that the Ga containing clathrate is thermodynamically more stable than the Al containing one. The calculated values of

TABLE I. Lattice constant, band gap, and formation energy E_f for $Ba_8Ga_{16}Sn_{30}$-VIII and $Ba_8Al_{16}Sn_{30}$-VIII. The previously reported empirical and theoretical values are also listed for comparison.

	Lattice constant (Å)			Band gap (meV)		E_f (kJ/mol)
Type-VIII Clathrate	Exp. (Ref. 73)	This work	Ref. 31	This work	Ref. 31	This work
$Ba_8Ga_{16}Sn_{30}$	11.58	11.93	11.88	160	190	−690
$Ba_8Al_{16}Sn_{30}$	…	11.92	…	315	…	−55.96

lattice constants, formation energies and fundamental band gaps for the clathrates of interest are listed in Table I. The reported empirical and theoretical values of the lattice constants and the band gaps have been presented in Table I for comparison.

B. Elastic properties

The elastic properties were calculated at the theoretical equilibrium volumes by setting the strain values equal to 0.005. The eigenvalues of the elastic stiffness matrix are positive-definite indicating that the clathrate crystals are mechanically stable. The eigenvalues are (30.28, 111.84, 20.28, 73.37, 73.37, 73.37) and (32.81, 113.44, 32.81, 57.52, 57.52, 57.52) for $Ba_8Ga_{16}Sn_{30}$-VIII and $Ba_8Al_{16}Sn_{30}$-VIII, respectively. Our calculated value of C_{44} (18.24 GPa) is comparable with the reported empirical value of 22.25 GPa at T = 0 K.[74] The calculated values of the elastic constants, bulk, shear, and Young's moduli, longitudinal, transverse, and mean sound velocities along with the Debye temperature for each compound are listed in Table II. As can be seen from Table II, replacing Ga atoms with Al in the framework does not lead to a significant change in elastic behavior of $Ba_8Ga_{16}Sn_{30}$-VIII and all the elastic properties remain almost unchanged. Therefore, both clathrates have similar stiffness against the uniform pressure, shearing strains and linear strain, which are measured, respectively, by bulk modulus, shear modulus and Young's modulus.

C. Phonon spectra and density of states

The lattice dynamics theory describes the collective motion of all atoms in the lattice by considering the vibrational eigenvalues or phonon spectra. Figs. 3(a) and 3(b) present our calculated ground state phonon dispersion curves at T = 0 K along with their corresponding vibrational densities of states (VDOS) for $Ba_8Ga_{16}Sn_{30}$-VIII and $Ba_8Al_{16}Sn_{30}$-VIII clathrates, respectively.

TABLE II. Elastic constants C_{ij}, bulk B, shear G, and Young's E moduli in GPa, longitudinal, transverse, and mean sound velocities in m/s, and the Debye temperature in K for $Ba_8Ga_{16}Sn_{30}$-VIII and $Ba_8Al_{16}Sn_{30}$-VIII.

Type-VIII Clathrate	$Ba_8Ga_{16}Sn_{30}$	$Ba_8Al_{16}Sn_{30}$
C_{11} (GPa)	57.37	59.76
C_{12} (GPa)	27.29	26.80
C_{44} (GPa)	18.24	14.46
B (GPa)	37.31	37.79
G (GPa)	16.89	15.23
E (GPa)	44.02	40.29
v_L (m/s)	3235	3368
v_T (m/s)	1719	1724
v_S (m/s)	1921	1932
θ_D (K)	181	182

Although the phonon spectra are similar to one another and share relatively common features, there are also some discrepancies. For example, for the case of the $Ba_8Al_{16}Sn_{30}$-VIII all energy gaps, especially the second one shown by the dark salmon band, are wider than those of the $Ba_8Ga_{16}Sn_{30}$-VIII. Moreover, below the second gap, the magnitude of VDOS for $Ba_8Al_{16}Sn_{30}$-VIII is significantly larger than that of $Ba_8Ga_{16}Sn_{30}$-VIII. The acoustic modes are located below approximately 0.37 and 1.1 THz for $Ba_8Ga_{16}Sn_{30}$-VIII and $Ba_8Al_{16}Sn_{30}$-VIII compounds, respectively, and the optic modes lie above that range. The acoustic mode curves have similar slopes indicating that the phonon group velocities or average speed of sounds in both compounds are very close to each other. Most of the optical mode curves are flat, which is reminiscent of the zone folding. The contribution of these modes to heat transport in the material is very small.[75] The highest optical modes are located in 6.382 and 9.17 THz for $Ba_8Ga_{16}Sn_{30}$-VIII and $Ba_8Al_{16}Sn_{30}$-VIII clathrates, respectively. An interesting feature of the calculated VDOS for the considered compounds is that it increases above acoustic branch. Moreover, the bandwidth of the heat-carrying acoustic

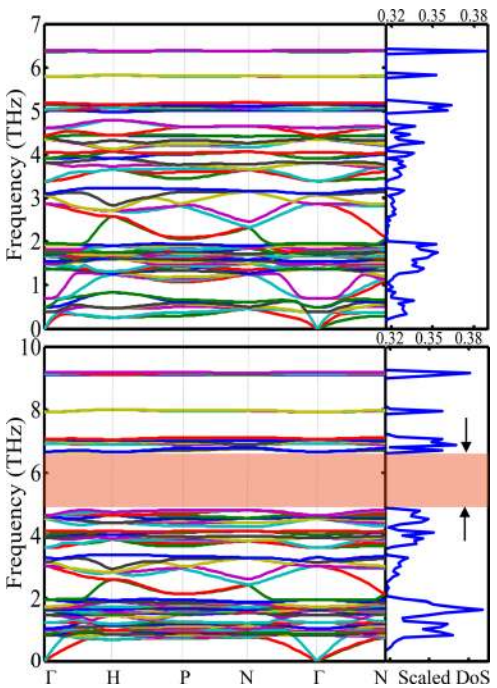

FIG. 3. The phonon dispersion curves and density of states for (a) $Ba_8Ga_{16}Sn_{30}$, and (b) $Ba_8Al_{16}Sn_{30}$. The k-points correspond to Γ = (0, 0, 0), H = (1/2, 1/2, -1/2), N = (1/2, 0, 0) and P = (1/4, 1/4, 1/4) in units of 2π/a.

modes in Al containing clathrate is larger than that of Ga containing one. In comparison to that of Al containing clathrate, the acoustic bandwidths in Ga containing clathrate is reduced by about 66%. The weak bonding of the guest atoms in the framework leads to low frequency localized vibrational modes of the guest atoms, which are coupled to the lattice modes and resonantly scatter the heat-carrying acoustic modes of the host framework.[76] Several flat vibrational bands can be observed in 0.66–0.7 and 1.38–1.95 THz regions for $Ba_8Ga_{16}Sn_{30}$-VIII and in 0.865 to 1.95 THz region (and at higher frequencies) for $Ba_8Al_{16}Sn_{30}$-VIII material. The non-dispersive feature of these optical modes shows major localization characters. These localized modes intersect the transverse and longitudinal acoustic (TA and LA) modes of the host atoms and there are strong interactions between the phonon modes. For example, crossings occur for the 0.381 flat along $N \rightarrow \Gamma$ and for the 0.818 THz flat along the same direction, respectively, in $Ba_8Ga_{16}Sn_{30}$-VIII and $Ba_8Al_{16}Sn_{30}$-VIII systems. These interactions cause the bending of the acoustic modes at several places in the Brillouin zone. This interaction is extended into optic regions for the LA modes. Avoided crossings of phonon modes with the same symmetry are responsible for these resonant interactions. This can potentially increase the probability of resonant scattering of the host acoustic phonons, and result in lower lattice thermal conductivity. In fact, symmetry avoided crossings lead to coupling of phonon modes which in turn dissipate the thermal energy of acoustic phonons to the localized vibrations of the guest atoms.[77,78] The phonon modes near the transition region of the acoustic to optic-mode range allow the thermal energy transfer from the framework to the guest atoms due to their dual nature.[45] We also found gaps in both phonon dispersion curves within the optic bands and VDOS. The gaps are located at about 3.22–3.44, 4.79–4.98, 5.2–5.80, and 5.82–6.39 THz ranges and 3.37–3.65, 4.8–6.65, 7.1–7.92, and 7.98–9.18 THz ranges for $Ba_8Ga_{16}Sn_{30}$-VIII and $Ba_8Al_{16}Sn_{30}$-VIII, respectively. The width of the second gap in $Ba_8Al_{16}Sn_{30}$-VIII is almost ten times wider than that of $Ba_8Ga_{16}Sn_{30}$-VIII. The existence of these gaps is a unique feature of the clathrates and is unusual in covalently bonded compounds. These gaps indicate that some spectral bands of phonons, which satisfy the Bragg condition, are filtered and are prevented from propagating. In

TABLE III. Frequencies and symmetry assignment of Raman and IR active modes at Γ point (symmetry T_d) in clathrates $Ba_8Ga_{16}Sn_{30}$-VIII and $Ba_8Al_{16}Sn_{30}$-VIII. R, I, and RI denote Raman, infrared and simultaneous Raman and infrared active modes, respectively.

$Ba_8Ga_{16}Sn_{30}$-VIII			$Ba_8Al_{16}Sn_{30}$-VIII		
Multiplicity	Frequency (THz)	Mulliken's symbol	Multiplicity	Frequency (THz)	Mulliken's symbol
3	0.0	T_2(RI)	3	0.0	T_2(RI)
3	0.380	T_1	3	0.817	T_1
2	0.492	E(R)	2	0.869	E(R)
3	0.697	T_2(RI)	3	0.993	T_2(RI)
3	1.373	T1	3	1.029	T1
1	1.378	A_1(R)	3	1.233	T_2(RI)
3	1.483	T_2(RI)	3	1.464	T_1
3	1.532	T_2(RI)	3	1.616	T_1
3	1.654	T_1	2	1.621	E(R)
3	1.698	T_2(RI)	3	1.633	T_2(RI)
2	1.745	E(R)	1	1.669	A_2
3	1.816	T_1	3	1.715	T_2(RI)
1	1.924	A_2	1	1.729	A_1(R)
3	1.957	T_2(RI)	3	1.944	T_2(RI)
3	2.864	T_1	3	3.011	T_1
1	3.062	A_1(R)	2	3.137	E(R)
2	3.096	E(R)	1	3.289	A_1(R)
3	3.387	T_2(RI)	3	3.598	T_2(RI)
3	3.805	T_2(RI)	3	3.917	T_2(RI)
2	3.907	E(R)	2	4.021	E(R)
1	4.053	A_1(R)	1	4.132	A_1(R)
3	4.348	T_1	1	4.525	A_1(R)
3	4.403	T_2(RI)	2	4.533	E(R)
1	4.436	A_1(R)	3	4.577	T_2(RI)
2	4.609	E(R)	3	4.635	T_1
3	5.007	T_1	3	6.661	T_1
3	5.039	T_2(RI)	3	6.923	T_2(RI)
3	5.144	T_1	3	7.033	T_2(RI)
3	5.187	T_2(RI)	3	7.050	T_1
3	5.780	T_2(RI)	3	7.912	T_2(RI)
1	6.359	A_2	2	9.106	E(R)
2	6.375	E(R)	3	9.131	T_2(RI)
3	6.389	T_2(RI)	1	9.167	A_2

TABLE IV. Irreducible representations of symmetry group T_d.

IR	1	5	7	9	11	6	8	10	12	2	3	4	38	39	43	44	46	48	37	40	41	42	45	47	Selections rules
A_1(R)	1	1	1	1	1	1	1	1	1	1	1	1	1	1	1	1	1	1	1	1	1	1	1	1	$x^2+y^2+z^2$
A_2	1	1	1	1	1	1	1	1	1	1	1	1	−1	−1	−1	−1	−1	−1	−1	−1	−1	−1	−1	−1	
E(R)	2	−1	−1	−1	−1	−1	−1	−1	−1	2	2	2	0	0	0	0	0	0	0	0	0	0	0	0	$(2z^2-x^2-y^2, x^2-y^2)$
T_1	3	0	0	0	0	0	0	0	0	−1	−1	−1	1	1	1	1	1	1	−1	−1	−1	−1	−1	−1	(J_x, J_y, J_z)
T_2(RI)	3	0	0	0	0	0	0	0	0	−1	−1	−1	−1	−1	−1	−1	−1	−1	1	1	1	1	1	1	(x,y,z), (xy, xz, yz)

molecular solids, the high energy intramolecular modes, which are caused by the framework atoms, are separated from the low energy intermolecular modes (guest-framework coupling modes), which results in these gaps.[79]

Lattice vibration at Γ point (symmetry T_d) can be described by Raman and infrared (IR) spectra. Raman and IR spectroscopy are well known methods to study atomic dynamics. So far, no empirical Raman and infrared spectra of clathrates $Ba_8Ga_{16}Sn_{30}$-VIII and $Ba_8Al_{16}Sn_{30}$-VIII have been reported to the best of our knowledge. From the group theory analysis, $Ba_8Ga_{16}Sn_{30}$-VIII has 23 Raman active modes (6E (R) + $4A_1$ (R) + $13T_2$ (RI)) and 13 infrared active modes ($13T_2$ (RI)). There exist also 22 Raman active modes (6E (R) + $4A_1$ (R) + $13T_2$ (RI)) and 13 infrared active modes ($13T_2$ (RI)) for $Ba_8Al_{16}Sn_{30}$-VIII. Therefore, though the frequency of Raman and IR active modes changes after Al substitution; however, the number of individual Raman and IR active modes remains unchanged. It is notable that simultaneous Raman and IR active modes occur only in non-centrosymmetric crystal structures. The calculated frequencies of Raman and infrared active modes at Γ point (symmetry T_d) are presented in Table III. We are not aware of any reported experimental or theoretical data of Raman and IR spectra for these materials; hence, a comparative analysis was not feasible.

The irreducible representations of symmetry group T_d have been demonstrated in Table IV.

D. Thermodynamic properties

The vibrational contributions to the specific-heat capacity, the entropy, and the Helmholtz free energy of $Ba_8Ga_{16}Sn_{30}$-VIII and $Ba_8Al_{16}Sn_{30}$-VIII clathrate materials were calculated in the temperature range of 0–450 C. This range was chosen according to the working temperature of these materials for thermoelectric applications. For example, n-type $Ba_8Ga_{16}Sn_{30}$-VIII has the maximum figure-of-merit of $ZT = 1.1$ at 400 C with carrier concentration of $n = 9.1 \times 10^{19}/cm^3$.[32] In theory of lattice dynamics, the specific heat at constant volume C_v is more easily calculated than specific heat at constant pressure C_p, which is generally measured in experiments. In solids the two quantities are related by $C_p - C_v = BTV\alpha^2$, in which α is the volume coefficient of thermal expansion, and B, T, and V are the bulk modulus, the absolute temperature, and the volume, respectively. Figures 4(a)–4(c) present the calculated temperature dependencies of the vibrational entropy, the specific heat at constant volume, and the vibrational Helmholtz free energy for $Ba_8Ga_{16}Sn_{30}$-VIII and $Ba_8Al_{16}Sn_{30}$-VIII materials. The temperature dependencies of all considered properties are qualitatively similar to each other for both these clathrates. Figure 4(a) shows our predicted temperature dependencies of the vibrational entropies for $Ba_8Ga_{16}Sn_{30}$-VIII and $Ba_8Al_{16}Sn_{30}$-VIII systems. The calculated vibrational entropies at T = 300 K are 1303 and 1225 J/Kmol, respectively, for $Ba_8Ga_{16}Sn_{30}$-VIII and $Ba_8Al_{16}Sn_{30}$-VIII systems. Replacing Ga atoms with Al slightly decreased the vibrational entropy. The vibrational entropy curves increase smoothly as temperature increases in the range of 0–450 K, which is an expected behavior because the vibrational frequencies increase with temperature. As can be seen in Figure 4(b), in the temperature range of 0–450 K, C_v presents typical Debye behavior and approaches to the Dulong and Petit value of $3NR$, where R is the gas constant, and N is the number of atoms in the unit cell. The C_v curve flattens out as the temperature increases above approximately 300 K. This indicates that the optic and acoustic modes of these clathrates are all excited at room temperature. According to

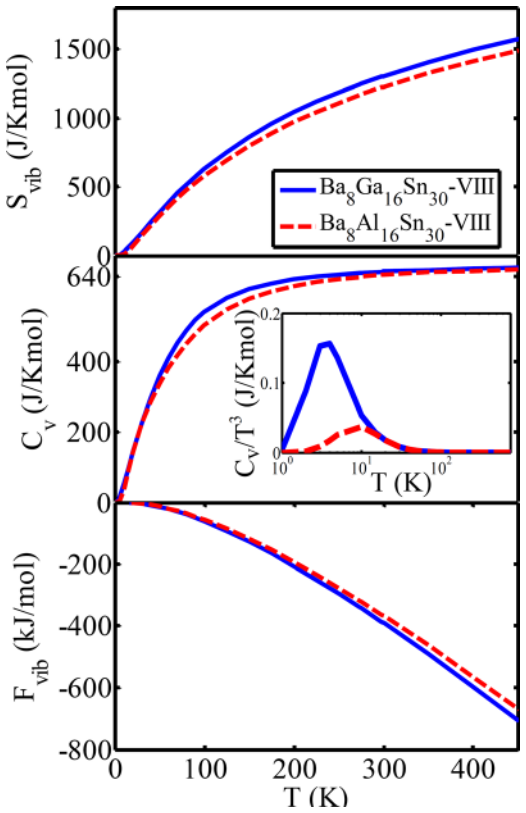

FIG. 4. Calculated thermal properties (a) vibrational entropy, (b) heat capacity at constant volume, and (c) vibrational free energy of $Ba_8Ga_{16}Sn_{30}$ and $Ba_8Al_{16}Sn_{30}$ in the temperature range of 0–450 K.

Figure 4(b), we predict that the Al substitution for Ga atoms in the framework has a negligible effect on the vibrational heat capacity. We find that at $T = 300\,K$, C_v for $Ba_8Ga_{16}Sn_{30}$-VIII and $Ba_8Al_{16}Sn_{30}$-VIII compounds is 655 and 645 J/Kmol, respectively. The inset depicts C_v/T^3 versus T for both $Ba_8Ga_{16}Sn_{30}$-VIII and $Ba_8Al_{16}Sn_{30}$-VIII compounds. The wide peaks in this plot indicate the anomalous rattling of the guest atoms or the Einstein-like vibrations, which is in good agreement with the empirical results.[20] Figure 4(c) plots the calculated results for the vibrational Helmholtz free energy, which is a geometry dependent quantity, as a function of temperature for $Ba_8Ga_{16}Sn_{30}$-VIII and $Ba_8Al_{16}Sn_{30}$-VIII compounds. Figure 4(c) predicts that the $Ba_8Ga_{16}Sn_{30}$-VIII clathrate is thermodynamically more stable than $Ba_8Al_{16}Sn_{30}$-VIII.

IV. SUMMARY AND CONCLUSION

In summary, the present work described the computational study of the structural, elastic, vibrational, and thermodynamic properties of $Ba_8Ga_{16}Sn_{30}$-VIII and $Ba_8Al_{16}Sn_{30}$-VIII clathrate compounds. GGA DFT was used to calculate a wide range of properties of the clathrates of interest and the results were presented. We selected zero Ga-Ga and Al-Al bond structures to construct the unit cell for $Ba_8Ga_{16}Sn_{30}$-VIII and $Ba_8Al_{16}Sn_{30}$-VIII clathrates and optimized the geometries of both considered clathrates. It was found that both clathrates have indirect band gaps. The predicted band gaps were approximately 160 meV and 315 meV, respectively, for $Ba_8Ga_{16}Sn_{30}$-VIII and $Ba_8Al_{16}Sn_{30}$-VIII clathrates. The effect of Al substitution for Ga in the framework on lattice constant and formation energy was investigated. The calculated elastic properties showed that the stiffness of $Ba_8Al_{16}Sn_{30}$-VIII against the uniform pressure, shearing strains and linear strain does not change significantly. The calculated phonon dispersion indicates that the Al substitution for Ga tends to widen the acoustic bandwidth of the framework; hence, potentially raising the lattice thermal conductivity. The calculated Raman and IR active phonon frequencies were reported by means of first principles calculations. Finally, we calculated the temperature dependencies of the vibrational entropy, vibrational specific heat, and the Helmholtz free energy for the clathrates of interest. According to our calculations, the temperature variations of these functions are similar to those found for other clathrate materials.[80–82]

ACKNOWLEDGMENTS

This work was partially supported by AFOSR under Grant No. FA9550-10-1-0010 and the National Science Foundation (NSF) under Grant No. 0933763. The authors would like to thank the Oklahoma State University's High Performance Computing center for many hours of computing time.

[1]G. S. Nolas, J. L. Cohn, G. A. Slack, and S. B. Schujman, Appl. Phys. Lett. **73**, 178 (1998).
[2]G. S. Nolas, J. Poon, and M. Kanatzidis, Mater. Res. Soc. Bull. **31**, 199–205 (2006).
[3]M. A. Avila, K. Suekuni, K. Umeo, H. Fukuoka, S. Yamanaka, and T. Takabatake, Phys. Rev. B **74**, 125109 (2006).
[4]H. Kawaji, H. O. Horie, S. Yamanaka, and M. Ishikawa, Phys. Rev. Lett. **74**, 1427 (1995).
[5]F. M. Grosche, H. Q. Yuan, W. C. Cabrera, S. Paschen, C. Langhammer, F. Kromer, G. Sparn, M. Baenitz, and G. Yu, Phys. Rev. Lett. **87**, 247003 (2001).
[6]A. San-Miguel, P. Kéghélian, X. Blase, P. Mélinon, A. Perez, J. P. Itié, A. Polian, E. Reny, C. Cros, and M. Pouchard, Phys. Rev. Lett. **83**, 5290 (1999).
[7]Y. Li and J. H. Ross, Appl. Phys. Lett. **83**, 2868 (2003).
[8]D. M. Rowe, *Thermoelectrics Handbook: Macro to Nano* (CRC Press 2005).
[9]J. Christofferson, D. Vashaee, A. Shakouri, and P. Melese, (ASME, New York, NY, 2001).
[10]X. Fan, G. Zeng, C. LaBounty, D. Vashaee, J. Christofferson, A. Shakouri, and J. E. Bowers, in *Proceedings of XX International Conference on Thermoelectrics (ICT)* (2001), IEEE Conference Publications, pp. 405–408.
[11]M. S. Dresselhaus, G. Chen, Z. F. Ren, J.-P. Fleurial, P. Gogna, M. Y. Tang, D. Vashaee, H. Lee, X. Wang, G. Joshi, G. Zhu, D. Wang, R. Blair, S. Bux, and R. Kaner, in Proceedings of the MRS Fall Meeting, November 26–30, Boston, MA, 2007, Paper No. U2.4 (invited paper presented by M. S. Dresselhaus).
[12]N. Satyala and D. Vashaee, Appl. Phys. Lett. **100**(7), 073107 (2012).
[13]Z. Zamanipour, X. Shi, A. M. Dehkordi, J. S. Krasinski, and D. Vashaee, Phys. Status Solidi A **209**(10), 2049–2058 (2012)
[14]D. Vashaee and A. Shakouri, Microsc. Thermophys. Eng. **8**(2), 91–100 (2004).
[15]D. Vashaee and A. Shakouri, J. Appl. Phys. **101**(5), 053719 (2007).
[16]D. Vashaee and A. Shakouri, "Improved thermoelectric power factor in metal-based superlattices," Phy. Rev. Lett. **92**(10), 106103-1 (2004).
[17]J. M. O. Zide *et al.*, "Demonstration of electron filtering to increase the Seebeck coefficient in In0.53Ga0.47As/In0.53Ga0.28Al0.19As superlattices," Phys. Rev. B: Condens. Matter Mater. Phys. **74**, 205335 (2006).
[18]D. Vashaee, Y. Zhang, A. Shakouri, G. Zeng, and Y. J. Chiu, Phys. Rev. B **74**(19), 195315 (2006).
[19]J. P. Heremans, V. Jovovic, E. S. Toberer, A. Saramat, K. Kurosaki, A. Charoenpakdee, S. Yamanaka, and G. Snyder, Science **321**, 554 (2008).
[20]S. Sumithra, N. J. Takas, D. K. Misra, W. M. Nolting, P. F. P. Poudeu, and K. L. Stokes, "Enhancement in thermoelectric figure of merit in nanostructured Bi_2Te_3 with semimetal nanoinclusions," Adv. Energy Mater. **1**, 1141–1147 (2011).
[21]Z. Zamanipour and D. Vashaee, J. Appl. Phys. **112**, 093714 (2012).
[22]G. J. Snyder and E. S. Toberer, "Complex thermoelectric materials," Nat. Mater. **7**(2), 105–114 (2008).
[23]G. A. Slack, *CRC Handbook of Thermoelectrics*, edited by D. M. Rowe (CRC Press, Boca Raton, FL, 1995), p. 407.
[24]J. L. Cohn, G. S. Nolas, V. Fessatidis, T. H. Metcalf, and G. A. Slack, Phys. Rev. Lett. **82**, 779–782 (1999).
[25]M. Volmer, C. Sternemann, J. S. Tse, T. Buslaps, and N. Hiraoka, Phys. Rev. B **76**, 233104 (2007).
[26]A. Saramat, G. Svensson, A. E. C. Palmqvist, C. Stiewe, E. Mueller, D. Platzek, S. G. K. Williams, D. M. Rowe, J. D. Bryan, and G. D. Stucky, J. Appl. Phys. **99**, 023708 (2006).
[27]L. Møllnitz, N. P. Blake, and H. Metiua, J. Chem. Phys. **117**, 1302 (2002).
[28]K. Suekuni, Y. Takasu, T. Hasegawa, N. Ogita, and M. Udagawa, Phys. Rev. B **81**, 205207 (2010).
[29]C. W. Myles, J. Dong, and O. F. Sankey, Phys. Rev. B **64**, 165202 (2001).
[30]C. W. Myles, J. Dong, O. F. Sankey, C. A. Kendziora, and G. S. Nolas, Phys. Rev. B **65**, 235208 (2002).
[31]D. C. Li, L. Fang, S. K. Deng, K. Y. Kang, L. X. Shen, W. H. Wei, and H. B. Ruan, Physica B **407**, 1238–1243 (2012).
[32]Y. Kono, N. Ohya, T. Taguchi, K. Suekuni, T. Takabatake, S. Yamamoto, and K. Akai, J. Appl. Phys. **107**, 123720 (2010).
[33]M. A. Avila, K. Suekuni, K. Umeo, H. Fukuoka, S. Yamanaka, and T. Takabatake, Appl. Phys. Lett. **92**, 041901 (2008).
[34]G. S. Nolas, J. L. Cohn, J. S. Dyck, C. Uher, G. A. Lamberton, Jr., and T. M. Tritt, J. Mater. Res. **19**, 3556 (2004).
[35]D. Huo, T. Sakata, T. Sasakawa, M. A. Avila, M. Tsubota, F. Iga, H. Fukuoka, S. Yamanaka, S. Aoyagi, and T. Takabatake, Phys. Rev. B **71**, 075113 (2005).
[36]Y. Kono, N. Ohya, Y. Saiga, K. Suekuni, T. Takabatake, K. Akai, and S. Yamamoto, J. Electron. Mater. **40**, 845 (2011).
[37]Y. Li, J. Gao, N. Chen, Y. Liu, Z. P. Luo, R. H. Zhang, X. Q. Ma, and G. H. Cao, Physica B **403**, 1140–1141 (2008).

[38]G. S. Nolas, J. L. Cohn, J. S. Dyck, C. Uher, and J. Yang, Phys. Rev. B **65**, 165201 (2002).
[39]B. C. Sales, B. C. Chakoumakos, R. Jin, J. R. Thompson, and D. Mandrus, Phys. Rev. B **63**, 245113 (2001).
[40]Y. Sasaki, K. Kishimoto, T. Koyanagi, H. Asada, and K. Akai, J. Appl. Phys. **105**, 073702 (2009).
[41]K. Kishimoto, N. Ikeda, K. Akai, and T. Koyanagi, Appl. Phys. Express **1**, 031201 (2008).
[42]S. Deng, Y. Saiga, K. Kajisa, and T. Takabatake, J. Appl. Phys. **109**, 103704 (2011).
[43]S. Deng, Y. Saiga, K. Suekuni, and T. Takabatake, J. Appl. Phys. **108**, 073705 (2010).
[44]S. Paschen, W. Carrillo-Cabrera, A. Bentien, V. H. Tran, M. Baenitz, Y. Grin, and F. Steglich, Phys. Rev. B **64**, 214404 (2001).
[45]We used the Vienna Ab initio Simulation Program (VASP), developed at the Institut für Theoretische Physik of the Technische Universität Wien. G. Kresse and J. Furthmüller, Comput. Mater. Sci. **6**, 15 (1996).
[46]G. Kresse and J. Hafner, Phys. Rev. B **47**, 558 (1993); G. Kresse and J. J. Furthmüller, *ibid.* **54**, 11169 (1996).
[47]J. P. Perdew, K. Burke, and M. Ernzerhof, Phys. Rev. Lett. **77**, 3865 (1996).
[48]D. Vanderbilt, Phys. Rev. B **41**, 7892 (1990); K. Laasonen, R. Car, C. Lee, and D. Vanderbilt, *ibid.* **43**, 6796 (1991).
[49]G. Kresse and J. Hafner, J. Phys.: Condens. Matter **6**, 8245 (1994); G. Kresse and J. Hafner, Phys. Rev. B **48**, 13115 (1993).
[50]H. J. Monkhorst and J. D. Pack, Phys. Rev. B **13**, 5188 (1976).
[51]F. Birch, J. Geophys. Res. **57**, 227, doi:10.1029/JZ057i002p00227 (1952).
[52]The Birch-Murnaghan equation for the energy E as a function of volume V is $E(V) = E_0 + 9/8(KV_0)[(V_0/V)^{2/3} - 1]^2 \{1 + [(4 - K')/2][1 - (V_0/V)^{2/3}]\}$.
[53]M. J. Mehl, J. E. Osburn, D. A. Papaconstantopoulos, and B. M. Klein, Phys. Rev. B **41**, 10311 (1990).
[54]A. V. Hershey, ASME J. Appl. Mech. Trans. **21**, 236 (1954).
[55]E. Kröner, Z. Phys. **151**, 504 (1958).
[56]R. Hill, Proc. Phys. Soc. London **65**, 349 (1952).
[57]L. Vitos, *Computational Quantum Mechanicals for Materials Engineers* (Springer-Verlag, London, 2007).
[58]H. M. Ledbetter, J. Appl. Phys. **44**, 1451 (1973).
[59]G. Grimvall, *Thermophysical Properties of Materials* (North-Holland, Amsterdam, 1999).
[60]K. Parlinski, Phonon Software Package, 2010.
[61]Y. Duan and D. C. Sorescu, Phys. Rev. B **79**, 014301 (2009).
[62]K. Parlinski, Z. Q. Li, and Y. Kawazoe, Phys. Rev. Lett. **78**, 4063 (1997).
[63]J. J. Dong, O. F. Sankey, G. K. Ramachandran, and P. F. McMillan, J. Appl. Phys. **87**, 7726 (2000).
[64]M. Menon, E. Richter, and K. R. Subbaswamy, Phys. Rev. B **56**, 12290 (1997).
[65]D. Connétable, Phys. Rev. B **75**, 125202 (2007).
[66]R. F. W. Herrmann, K. Tanigaki, S. Kuroshima, and H. Suematsu, Chem. Phys. Lett. **283**(1), 29–32 (1998).
[67]B. Eisenmann, H. Schafer, and R. Zagler, J. Less-Common Met. **118**, 43 (1986).
[68]S. Leoni, W. Carrillo-Cabrera, and Y. Grin, J. Alloys Compd. **350**, 113 (2003).
[69]S. Y. Rodriguez, X. Zheng, L. Saribaev, and J. H. Ross, Jr., Proc. Mater. Res. Soc. **1267**, DD04–07 (2010).
[70]N. P. Blake, D. Bryan, S. Latturner, L. Mollnitz, G. D. Stucky, and H. Metiu, J. Chem. Phys. **114**, 10063 (2001).
[71]W. Gou, S. Y. Rorigues, Y. Li, and J. H. Ross. Jr., Phys. Rev. B **80**, 144108 (2009).
[72]V. N. Staroverov *et al.*, Phys. Rev. B **69**, 075102 (2004).
[73]T. Iitaka, Phys. Rev. B **75**, 012106 (2007).
[74]I. Ishii, H. Higaki, T. Sakata, D. Huo, T. Takabatake, and T. Suzuki, Physica B **359–361**, 1210–1212 (2005).
[75]N. W. Ashcroft and N. D. Mermin, *Solid State Physics* (Holt, Reinhart, and Winston, New York, 1976), p. 500.
[76]G. S. Nolas, G. A. Slack, and S. B. Schujman, *in Recent Trends in Thermoelectric Materials Research I, Semiconductors and Semimetals*, edited by T. M. Tritt (Academic, San Diego, 2000), Vol. 69 and references therein.
[77]J. S. Tse *et al.*, J. Chem. Phys. **107**, 9271 (1997).
[78]J. S. Tse, J. Inclusion Phenom. **17**, 259 (1994).
[79]D. Kahn and J. P. Lu, Phys. Rev. B **56**, 13898 (1997).
[80]A. Bentien, S. Johnsen, and B. B. Iversen, Phys. Rev. B **73**, 094301 (2006).
[81]L. Qiu, I. P. Swainson, G. S. Nolas, and M. A. White, Phys. Rev. B **70**, 035208 (2004).
[82]L. Qiu, M. A. White, Z. Li, J. S. Tse, C. I. Ratcliffe, C. A. Tulk, J. Dong, and O. F. Sankey, Phys. Rev. B **64**, 024303 (2001).